Testing the impact of stratigraphic uncertainty on spectral analyses of sedimentary series

Martinez Mathieu[1], Kotov Sergey[1], De Vleeschouwer David[1], Pas Damien[2], and Pälike Heiko[1]

[1]MARUM – Centrum for Marine Environmental Sciences, Leobenerstr., Universität Bremen, D-28359, Germany
[2]Pétrologie sédimentaire, B20, Géologie, Université de Liège, Sart Tilman, B-4000 Liège, Belgium

Correspondence to: Mathieu Martinez (mmartinez@marum.de)

Abstract. Spectral analysis is a key tool for identifying periodic patterns in sedimentary sequences, including astronomically related orbital signals. While most spectral analysis methods require equally-spaced samples, this condition is rarely achieved either in the field or when sampling sediment cores. Here, we propose a method to assess the impact on the resulting power spectra of the uncertainty or

5 error made in the measurement of sample stratigraphic position. We apply a Monte-Carlo procedure to randomise the sample steps of depth series using a gamma distribution. Such a distribution preserves the stratigraphic order of samples, and allows control of the mean and variance of the sample step distribution after randomisation. We test the Monte-Carlo procedure on two geological datasets and find that at 5% uncertainty in the sample positions, the power of the spectral peaks is signifi-

10 cantly affected in all frequencies above ~1/3 of the Nyquist frequency. The randomisation process progressively affects the lower frequencies when increasing the level of uncertainty in the sample position. With 10% sample position uncertainty, the change in relative power exceeds 10% in all frequencies above ~1/5 of the Nyquist frequency. For robust applications of the power spectrum, we suggest strongly controlling the measurement of the sample position, keeping the variance of the

15 sample distribution to a maximum of 10% of the average sample step. In addition, the simulations indicate that taking at least 6-10 samples per precession cycle should allow calculation of robust power spectra estimates in the Milankovitch band.

1 Introduction

Spectral analysis methods have become a key tool for identifying Milankovitch cycles in sedimentary

20 series and are a crucial tool in the construction of robust astronomical time scales (Hinnov, 2013). The climatic or environmental proxy series that form the subject of spectral analyses are generally the result of measurements on rock samples collected from a sedimentary sequence, consisting of cores or outcrops. Most of spectral analysis methods (Fourier Transforms and derivatives, such as the Multi-Taper Method) require equally-spaced depth- or time-series, which implies that samples

25 need to be taken at a constant sample step. Unfortunately, this is rarely achieved, especially for sedimentary sequences sampled in outcrops. Often, an uncertainty of ~5-15% is observed in the thickness or distance measurements, even when using a Jacob's staff (Weedon and Jenkyns, 1999). In core sediments, uncertainties in the sample position are also observed when performing physical sampling at very high resolution or because of core expansion phenomena (Hagelberg et al., 1995).

30 Although uncertainties exist on the actual position of samples, few case studies document their effect on the identification of periodic patterns. Moore and Thomson (1991) recognised that perturbations of the regular sampling scheme (i.e. jittered sampling) impact the power spectrum by reducing spectral power in the high frequencies. Huybers and Wunsch (2004) and Martinez and Dera (2015) address an analogous problem by assessing the effect of sampling uncertainty on the age model of

35 a calibrated time series that is plotted against numerical age. However, none of these studies explicitly addresses the impact of errors in the measurement of the sample position on uncertainties in the power spectrum amplitudes. In this study, we address this problem by quantifying the impact of such errors on the frequency, as well as the power of higher-frequency cycles. Therefore, we provide a new procedure that is based on a Monte-Carlo approach for sample step randomisation. The

40 randomised sample steps are subsequently used to assess the impact of the sample-position error on spectral analyses. We first apply the procedure to a theoretical example, and then to two previously published geological datasets: 1) sampled as regularly as possible and 2) sampled irregularly. Based on our results, we suggest that one should take at least ~10 measurements per high-frequency cycle in order to provide robust estimates of the power of the high-frequency cycles.

45 ## 2 The error model

In this paper, the term "stratigraphic uncertainty" refers to the uncertainty in the sample positions. Testing the impact of the stratigraphic uncertainty on the spectral analyses requires a randomisation procedure that correctly reflects typical errors made during measurements of the stratigraphic position of samples. Therefore, two conditions must be respected: (i) the stratigraphic order of samples

50 is fixed and should not be changed by the randomisation process, (ii) the average and standard deviation of sample steps should be maintained during the randomisation process. Both conditions can be achieved if the error model randomises the sample distances rather than the sample positions. In that case, the probability density function should have a positive and continuous distribution (i.e. values obtained after randomisation are continuous and positive). In addition, the average sample step and

55 the standard deviation of the distance between two successive samples are known and parameterized. The gamma distribution fulfils all these conditions. The gamma distribution is continuous and has a positive support. Parameters k and Θ respectively define the shape of the distribution and its range of values. The mean (E) of the density of probability is defined as (Burgin, 1975):

$$E = k * \Theta \tag{1}$$

and its variance (σ^2)

$$\sigma^2 = k * \Theta^2 = E * \Theta \tag{2}$$

Both the mean (E) and the variance (σ^2) are known, as they correspond to the mean and variance of the sample steps, and they can be quantified in the field (see Section 4 for a discussion on the variance of sample steps). Therefore, k and Θ can easily be parameterized using the following relations:

$$\Theta = \frac{\sigma^2}{E} \tag{3}$$

$$k = \frac{E}{\Theta} \tag{4}$$

Various gamma probability density functions are shown in Figure 1. A high variance-to-mean ratio corresponds to a high Θ-parameter value compared to the k-parameter. The resulting density probability function corresponds to an exponential probability function in the most severe and spectrum-destructive case. This distribution corresponds to sampling conditions during which no control was exerted on the stratigraphic position of samples, so that the uncertainty on the sample position is at a maximum. Obviously, this situation is not a realistic case of geological practice. In the opposite case, a low variance-to-mean ratio corresponds to a low Θ-parameter value compared to the value of the k-parameter. The resulting density probability function is close to a Gaussian curve, although bound on one side to 0, so that the curve has a positive support. This case corresponds to geological sampling during which the position of each sample was carefully measured and reported with respect to the stratigraphic column. Nevertheless, even in this case, stratigraphic uncertainties are unavoidable, mainly because of outcrop or core conditions.

3   The geological datasets

Two published geological datasets were used here to assess the effect of stratigraphic uncertainty on power spectra.

3.1   Gamma-ray spectrometry from La Charce (Valanginian, Early Cretaceous)

A total of 555 gamma-ray spectrometry measurements were performed *in situ* on the La Charce section (Department of Drôme, SE France; Martinez et al., 2013, 2015). The section is composed of marl-limestone alternations that were deposited in a hemipelagic environment during the Valanginian and Hauterivian stages (~134-132 Ma, Early Cretaceous; Martinez et al., 2015). Detailed analyses of the clay mineralogical, geochemical, and faunal contents indicated that these alternations reflect orbital climate forcing. Gamma-ray spectrometry measurements were used to identify the precession, obliquity and 405-kyr eccentricity cycles (see Martinez et al., 2015).

Gamma-ray spectrometry measurements were performed directly in the field with an as regular as possible sample step of 0.20 m. Before each measurement, rock surfaces were first cleaned to remove reworked material and flattened to prevent any border effects that could affect the measurement value. Each measurement was performed using a SatisGeo GS-512 spectrometer, with a constant acquisition time of 60 seconds (more details are provided in Martinez et al., 2013). The raw data are available in the following link: http://www.sciencedirect.com/science/article/pii/S0031018213000977.

3.2 Magnetic susceptibility from La Thure section (Givetian, Middle Devonian)

The second case study consists of the 184-m-thick continuous early-Givetian to early-Frasnian sequence of the La Thure section. The Givetian sequence is composed of bedded limestone, mainly deposited in a shallow-water rimmed-shelf characterised by a large set of internal and external rimmed-shelf environments (Pas et al. in press). The overlying early Frasnian sequence is dominated by shale deposited in a siliciclastic drowned platform (Pas et al., 2014). The magnetic susceptibility (MS) data from the La Thure section, in combination with three other MS datasets from the Dinant Syncline in southern Belgium and northern France were used by De Vleeschouwer et al. (2014) to make an estimate of the duration of the Givetian Stage, and subsequently to calibrate the Devonian time scale (De Vleeschouwer and Parnell, 2014). Spectral analysis of the MS data from the La Thure section revealed the imprint of different Milankovitch astronomical parameters, including eccentricity, obliquity and precession (Fig. 3C in De Vleeschouwer et al. (2014)). A total of 484 samples were taken along the 184-m thick sequence, with an irregular sample step that varied between 20-45 cm, depending on outcrop conditions (average sample step: 38 cm). Magnetic susceptibility measurements were performed using a KLY-3S instrument (AGICO, noise level $2*10^{-8}SI$) at the University of Liège (Belgium) (more details provided in De Vleeschouwer et al., 2014). The raw data are provided in the following Pangaea link: http://doi.pangaea.de/10.1594/PANGAEA.855764.

4 Implementation of the models in the stratigraphic-uncertainty tests

Weedon and Jenkyns (1999) estimated the error on the stratigraphic position of a sample to be 5.3% by measuring the thickness of the same sequence twice. The La Charce section, one of the datasets treated here, has been measured multiple times in different publications. The thickness of the studied section was assessed at 106 m, 109 m and 116 m (Bulot et al., 1992; Martinez et al., 2013; Reboulet and Atrops, 1999) with an average of 110.3 ± 5.1 m, and a relative uncertainty of 4.6% in the total thickness of the series. In the field, the distance between two successive samples was measured independently from the construction of the log, providing an independent assessment of the distribution of the actual distance between two successive samples. The average sample step is 20 cm, with a standard deviation of the sample steps of 2.5 cm, which corresponds to an uncertainty of 12.5% in the average sample step.

125   Based on the assessments summarised in the previous paragraph, we tested three different levels
for the error on the measurement of sample steps (5%, 10% and 15%), which we consider realistic
scenarios for geological sampling during fieldwork. We applied our Monte-Carlo based procedure
for randomising sample steps to a sinusoidal series, as well as to the two previously-published ge-
ologic datasets described in section 3 (De Vleeschouwer et al., 2014; Martinez et al., 2013, 2015),
130   with three different error levels. During every Monte-Carlo simulation, the distance between two
points is randomised according to a gamma distribution, of which the mean corresponds to the dis-
tance between two points measured in the field, and of which the standard deviation corresponds
to 5%, 10% or 15% of the measured distance. Each test consists of 1000 Monte-Carlo simulations,
leading to 1000 different time series, each with a different distortion of the stratigraphic positions of
135   samples.

Spectral analyses were performed using the Multi-Taper Method (MTM; Thomson, 1982, 1990),
using three 2π-tapers (2π-MTM analysis) and with the Lomb-Scargle method (Lomb, 1976; Scar-
gle, 1982). For the 2π-MTM analysis, confidence levels of the spectra of the original geological
datasets tested were calculated using the Mann and Lees (1996) approach (ML96), with median-
140   smoothing calculated with the method of the Tukey's end point rule, as suggested by Meyers (2014).
The window width for the median-smoothing was fixed at 20% of the Nyquist Frequency, as evalu-
ated empirically by Mann and Lees (1996). As MTM analysis requires strictly regular sample steps,
the geological datasets were linearly interpolated at 0.01 m before and after randomisation. The sum
of sinusoid series is generated with a regular sample step of 1 arbitrary unit. After randomisation,
145   the depth-randomised series was linearly interpolated at 1 arbitrary unit.

Lomb-Scargle spectra were calculated with the REDFIT algorithm (Schulz and Mudelsee, 2002).
The Lomb-Scargle method calculates the spectrum of unevenly-sampled series. Lomb-Scargle power
spectra can be biased in the high frequencies due to the non-independency of the frequencies (Lomb,
1976; Scargle, 1982); however, the REDFIT algorithm corrects the power spectrum by fitting a red-
150   noise model to the spectrum (Mudelsee, 2002; Schulz and Mudelsee, 2002). Here, we applied no
segmentation to the series and a rectangular window. This parameterization maximises the effect of
sample step randomisation on the spectrum.

During each test, both MTM and REDFIT Lomb-Scargle power spectra were calculated for each
of the 1000 Monte-Carlo distorted series. Subsequently, the average MTM and Lomb-Scargle spectra
155   were calculated. The confidence levels of the datasets were calculated before randomisation and
directly plotted to the simulated spectra. The sum of sinusoids series does not need correction for
red noise and the raw Lomb-Scargle spectra are shown. The two geological datasets show a red-noise
background and the REDFIT-corrected Lomb-Scargle spectra were shown.

Finally, we provide a quantification of the relative change in spectral power, using the following
160   criterion:

$$E_r(f) = \left| \frac{P_{ori}(f) - P_{ave}(f)}{P_{ave}(f)} \right| \tag{5}$$

with f: the frequencies explored in the spectral analyses, E_r: the relative change of power, P_{ori}: the power spectrum before randomization, and P_{ave}: the average power spectrum of the 1000 simulations.

5 Application to a sum of sinusoids

The effect of randomising the sample position within the section is first tested on a sum of pure sinusoids. A dataset of 600 points is generated with a sample step of 1 arbitrary unit. The series is a sum of 24 sinusoids, having equal amplitudes and different frequencies: frequencies range from 0.02 to 0.48 cycles/arbitrary unit and increase with increments of 0.02 cycles/arbitrary unit (Fig. 2A). Figures 2B to 2D show, in grey, the 2π-MTM spectra of 1000 Monte-Carlo randomisations of the sample step in this depth series, with a standard deviation ranging from 5 to 15% of the average sample step. The average spectrum of these simulations is shown with 5% uncertainty (orange - Fig. 2B), 10% uncertainty (red - Fig. 2C), and 15% uncertainty (brown - Fig. 2D). The most striking feature after gamma-model randomisation is the progressive and strong decrease of the powers towards the high frequencies, even when the lowest level of uncertainty (5%) is considered. Notably, for 5% uncertainty in sample position, a 10% reduction in power of the spectral peaks is observed in all frequencies above 24% of the Nyquist frequency, while at 50% of the Nyquist frequency the power of the peaks is reduced by more than 40% (Fig. 2E). For 10% and 15% uncertainty, a 10% reduction in power of the peaks is respectively observed in all frequencies above 16% and 12% of the Nyquist frequency, while at 50% of the Nyquist frequency the power of the peaks is reduced by respectively 60% and 73% (Fig. 2E).

The tests of the Lomb-Scargle spectra (Fig. 3) shows a 10% decrease power (i) in all frequencies above 32% of the Nyquist frequency in the 5%-uncertainty test, (ii) above 16% of the Nyquist frequency in the 10%-uncertainty test and (iii) above 12% of the Nyquist frequency in the 15%-uncertainty test. In the 5%-uncertainty test, the first significant change in power occurs at a higher frequency in the Lomb-Scargle spectrum than in the MTM spectrum. At 10% and 15% uncertainty, the first frequency at which the relative change in power exceeds 10% is the same in both the Lomb-Scargle and the MTM spectra (Figs. 2 and 3).

The sample step randomisation distorts the distances between two successive points (Figs. 2F-2H). The periods of the original signal are thus distorted, triggering a dispersion of the power spectrum on a large set of frequencies. In the original sum of sinusoid series, the power spectrum is concentrated on the frequencies of the sinusoids (Fig. 2A). After sample step distortion, part of the power spectrum of these frequencies is shifted to the surrounding frequencies (Fig. 2B-2D). Consequently, we observe on the spectrum (i) a decrease in the average power spectrum at the frequencies of the series before randomisation and (ii) an enhancement of the average power spectrum of the surrounding frequencies. The lowest frequencies are much less affected by sample step randomisation, because a

strong change in periods is needed to shift from a frequency to another in the lowest frequencies. In the high frequencies, small changes to the period are sufficient to cause frequency shift. The higher the error on the sample step, the stronger the dispersal of the distances between two successive points (Figs. 2F to 2H), and the more the lowest frequencies are impacted. Differences in the first frequency showing significant relative change in power are only observed between the Lomb-Scargle and the MTM spectra at 5% uncertainty. The difference between the two methods may be due to the resampling procedure, required in the MTM analysis, that reduces the amplitude of cycles documented by less than 5 points (Hinnov et al., 2002).

It should be noted that in the case of pure sinusoids, the signal is only composed of pure harmonics that concentrate the spectral power at specific frequencies. Therefore, a small shift in the sample position triggers a strong decrease of the average power spectrum at these specific frequencies. In addition, in this theoretical example, the sampling step was strictly constant before randomisation (1 arbitrary unit). More realistically, geological datasets are not strictly evenly sampled, and their spectra are rather composed of a mixture of harmonics, narrow-band and background components. In the following section, the results of the test on two geological datasets are shown.

6 Application to geological datasets

6.1 Gamma-ray series from La Charce

The raw gamma-ray series from La Charce is demonstrated in the black curve in Figure 4A, while the red curve shows a random sample step simulation performed by fixing a standard deviation of the distribution of the sample steps at 15% of the average sample step. This comparison shows (i) that the stratigraphic order of the samples in the raw series is preserved after randomisation and (ii) that the maximum difference in the stratigraphic position of a specific sample between the raw and the randomised curve is a few meters, even with the strongest dispersion of the sample steps tested here. This difference realistically simulates small thickness errors, which accumulate when measuring successive sample steps.

Prior to performing 2π-MTM analyses, the gamma-ray series (raw and sample-position randomised) was linearly interpolated at 0.01 m, detrended using a best-fit linear regression and standardised to zero average and unit variance. Prior to REDFIT Lomb-Scargle analysis, the datasets (raw and randomised) were simply linearly detrended using a best-fit linear regression and standardised.

The 2π-MTM analysis of the La Charce section shows two main significant bands at 20 m and from 1.3 to 0.8 m (>99% Confidence Level, hereafter abbreviated CL; Fig. 4C). A final low-power peak at 0.7 m exceeds the 95% CL. In previous cyclostratigraphic studies, the peak of 20 m was interpreted as the imprint of 405-kyr eccentricity forcing, while the peaks of 1.3 to 0.7 m were predominantly attributed to precession forcing (Boulila et al., 2015; Martinez et al., 2013, 2015).

The REDFIT spectrum shows two bands of periods exceeding the 99% CL at 18 m and from 1.4 to 0.8 m. The peak at 0.7 m observed in the MTM analysis exceed the 90% CL in the REDFIT spectrum. These periods are similar to the periods observed in the 2π-MTM spectrum. The small

235   differences in periodicity observed in the lowest frequencies are likely to be related to the difference in frequencies explored between both methods. In addition, the REDFIT spectrum, as parameterised here, produces narrower peaks than the multi-taper spectrum. Therefore, the lowest frequencies in the REDFIT spectrum are composed of a group of narrow peaks, whereas a single broad peak is observed in the 2π-MTM spectrum.

240   After randomisation with a standard deviation fixed at 5% of the average sample step, significant changes in power occur in frequencies above 40% of the Nyquist frequency in the 2π-MTM spectrum (Fig. 5G), and above 34% of the Nyquist frequency in the REDFIT spectrum (Fig. 6G). At 5% uncertainty, the peak at 0.7 m does not exceed the 90% CL in the REDFIT spectrum (Fig. 6A), while it still reaches the 95% CL in the 2π-MTM spectrum (Fig. 5A). Generally, the spectra of the series

245   after randomisation with 5% uncertainty are similar with the spectra before randomisation in the Milankovitch band. Only the last third of the spectra are smoothed compared to the original series (Figs. 5D, 6D). At σ=10% and 15%, significant changes in the power spectrum respectively occur in frequencies above 24% and 19% of the Nyquist frequency in the 2π-MTM spectrum (Figs. 5H-I), while such changes occur respectively from 20% and 19% of the Nyquist frequency in the REDFIT

250   spectrum (Figs. 6H-I). The average spectra are significantly smoothed in the precession band in both the 2π-MTM and the REDFIT spectra (Figs. 5E-F, 6E-F). Notably at σ=15%, the significant peak at 0.8 m in the spectra of the raw series appears as simple shoulder of a peak at 1 m (Figs. 5C, 6C). On average, a decrease in spectral power of 25% in the MTM spectrum and of 50% in the REDFIT spectrum is commonly observed in the precession band for the test with σ fixed at 15% of the average

255   sample step (Figs. 5I, 6I).

6.2 Magnetic susceptibility from La Thure

The magnetic susceptibility signal from La Thure is shown in Figure 4B in black together with a series with randomised sample step in red. As in the case of the La Charce series, the stratigraphic order of the samples is preserved in the randomised series. The difference in the stratigraphic posi-

260   tion of a specific sample between the raw and the randomised curve locally amounts several meters, realistically simulating the cumulative thickness errors on the measurement of sample positions in the field. Prior to 2π-MTM analysis, the randomised datasets were linearly interpolated at 0.01 m. The long-term trend of the mean was removed from the series by subtracting a piecewise best-fit linear regression. The long-term trend of the variance was then removed by dividing the series by

265   the instantaneous amplitude smoothed with a LOWESS regression with a 10% coefficient. This approach allows the series to have a stationary mean and variance. The series was subsequently stan-

dardised (average=0; standard deviation=1). Prior to the REDFIT analysis, the identical procedure
was applied, except for the linear interpolation, as this is not required by the Lomb-Scargle method.

The 2π-MTM analysis of the La Thure section shows significant periods at 36 m (>95% CL)
interpreted as the manifestation of the 405-kyr eccentricity cycle (De Vleeschouwer et al., 2014),
at 7.9 m (>99% CL) interpreted as 100-kyr eccentricity cycles, a group of significant periods from
2.8 m to 2.2 m (>99% CL) interpreted as obliquity, and a group of significant periods from 1.7
to 1.1 m (>99% CL) interpreted as precession (Fig. 4D). In the lowest frequencies, the REDFIT
spectrum (Fig. 4F) shows a group of peaks centred on 30-40 m (>99% CL), a peak at 14 m (>95%
CL), which is not significant in the 2π-MTM spectrum. Conversely, the period at 7.9 m observed
in the 2π-MTM spectrum does not reach the 90% CL in the REDFIT spectrum. These differences
are likely related to the difference in the frequencies explored between both methods, to the fact that
REDFIT spectra as parameterised here produce narrower peaks than the 2π-MTM spectra, and to
the different approaches to calculate the red-noise background (Meyers, 2014; Mudelsee, 2002). In
the REDFIT spectrum, the obliquity band shows three periods at 3.3 m (>90% CL), 2.6 m (>90%
CL) and 2.3 m (>95% CL). The precession band shows periods at 1.5 m (>90% CL), 1.2 m (>95%
CL), 1.1 m (>99% CL) and at 0.9 m (>99% CL). Generally, the precession and obliquity bands show
lower confidence levels than with the 2π-MTM spectrum, likely because of the different approach
to calculate the red-noise background.

After randomisation with a standard deviation fixed at 5% of the average sample step, significant
changes in power occur in frequencies above 34% of the Nyquist frequency in the 2π-MTM spectrum
(Fig. 7G), and above 38% of the Nyquist frequency in the REDFIT spectrum (Fig. 8G). In the
REDFIT spectrum, the peak at 0.9 m does not exceed the 95% CL after randomisation (Fig. 8A).
At 10% uncertainty in the sample step, significant change in power occur in frequencies above 23%
of the Nyquist frequency in the 2π-MTM spectrum, and above 21% in the REDFIT spectrum (Figs.
7H, 8H). In the 2π-MTM spectrum, the peak at 1.2 m is hard to distinguish from the background
(Figs. 7B, 7E). In the REDFIT spectrum, the precession is also greatly smoothed and no peak in
this band reaches the 95% CL (Figs. 8B, 8E). Finally, at 15% uncertainty in the sample step, 10%
of relative change in power is reached in frequencies above 14% of the Nyquist frequency in the
2π-MTM spectrum, and above 15% of the Nyquist frequency in the REDFIT spectrum (Figs. 7I,
8I). In both methods, the spectral peaks in the precession are flattened (Figs. 7C, 7F, 8C, 8F). In the
obliquity band, the amplitudes of the peak are significantly reduced.

7   Discussion

7.1   Comparison of the results between the two geological datasets

Although the 2π-MTM and REDFIT spectra do not show exactly the same power and main signifi-
cant periods, the relative change in power shows a similar behaviour between the two methods and

between the two geological datasets for a same fixed standard deviation of the average sample step. In all cases, the spectral power values at high frequencies are more affected than at low frequencies, and increasing uncertainty in the sample position increases the relative change in powers.

305   In particular at 5% uncertainty, a 10% relative change in power occurs -on average- at 37% of the Nyquist frequency. An uncertainty of about 5% is commonly observed in the thickness measurement of outcrop sections (see section 4), even when using a Jacob's staff (Weedon and Jenkyns, 1999). An uncertainty lower than 5% is very hard to achieve and, therefore, we suggest applying 5% uncertainty as the lowest level of uncertainty that can be reached when working on real geological data.

310   The above-presented result suggest that precession-related peaks in the power spectrum should be at a frequency that is lower than ~1/3 of the Nyquist frequency in order to obtain a robust detection of the full Milankovitch band. This requires that more than 6 samples per precession cycle have to be taken. Actually, 6 samples per astronomical cycle should be considered the lowest sampling density, since all tests carried out in the framework of this paper show that at 5% uncertainty, significant

315 dispersion of spectral power occurs at frequency higher than ~1/3 of the Nyquist frequency. Hence, the high-frequency portion of the spectrum should be interpreted with much caution. At 10% uncertainty, all analyses show a threshold of significant relative change in power at 22% of the Nyquist frequency, with very little difference between the four methods (20% to 24%; Figs. 5 to 8). The results indicate that significant changes in power occur in frequencies above ~1/5 of the Nyquist fre-

320 quency, suggesting that taking a minimum of 10 samples per precession cycle is required to prevent strong biases in the power estimates for the Milankovitch frequency band.

7.2   When to apply this test?

Uncertainties in the measurement of sample position can practically not be avoided in outcrop conditions. The similarity between the topographic slope and the sedimentary dip, the absence or scarcity

325 of marker beds, or the need to move laterally in a section can trigger disturbances in the sampling regularity. In core sedimentary sequences, non-destructive automated measurements such as X-ray fluorescence, gamma-ray spectrometry or magnetic susceptibility should prevent errors in the sample position. However, physical samplings (e.g. for geochemistry or mineralogy) are subject to small uncertainties, especially when the sampling resolution is very high. Core sedimentary series can in

330 addition be affected by expansion of sediment caused by release of gas or release of overburden pressure (Hagelberg et al., 1995). This test is thus useful for geologists who wish to run spectral analyses on sedimentary depth-series generated from outcropping sections or core samples. All analyses in this paper show that with higher uncertainty on the sample step, the low frequencies are increasingly affected. The relative change in power between the various tests all showed different patterns, and

335 no general model could be deduced. The relative change in power at a given frequency depends on the dispersion of the sample step, on the method of spectral analysis, but also on the original sedimentary sequence studied. Each depth-series generated from this sampling can be seen as one

of the 1000 random simulations. The test randomises the sample position from the original series, and produces a smooth version of the spectrum of the raw series. The generation of the raw series

340   impacts on the test at frequencies having low powers (a small change in a weak power can trigger high values of relative change in power), and at high frequencies. The relative change in power does not depend on the size of the sample step itself, as the same proportion of the spectrum is affected for a given level of uncertainty. However, a control on the dispersion of the sample steps and the application of the test proposed here are needed to assess the dispersion of the sample step during

345   the sampling procedure and the impact of this dispersion on the spectrum. The question is how to assess the dispersion of the sample step in the field? If the section is well bedded, we suggest applying the same procedure as we did for La Charce, i.e. sample position measured independently from the bed thickness measurements, and a precise report of the sample positions on the sedimentary log of the series. Orbital forcing can also be detected in a monotonous thick marly section, showing

350   no apparent bedding (e.g., Ghirardi et al., 2014; Matys Grygar et al., 2014). In that case, we rather suggest measuring the total thickness of the sequence several times to assess the potential dispersion of the sample steps.

7.3   Implications for astronomical time scale and palaeoclimate reconstructions

Linking sedimentary cycles to orbital cycles or assessing the quality of an orbital tuning procedure

355   often require the determination of the amplitude modulation of the orbital cycles (Moiroud et al., 2012; Zeeden et al., 2015). Stratigraphic uncertainties trigger a decrease of the power spectrum of the main significant frequencies while distributing the power spectrum to the surrounding frequencies. Thus, a filter, if designed very narrowly, can lead to a distortion of the actual amplitude of the filtered frequency. This is particularly critical for the precession band, which has been proven to be

360   sensitive to stratigraphic uncertainty (Figs. 5 to 8), and for which amplitude modulation is governed by eccentricity. Note than the procedure of Zeeden et al. (2015) is based on a wide filter, so that the biases triggered by stratigraphic uncertainty on their test should be limited. Otherwise, a robust reconstruction of the amplitude modulation of the precession band requires limited biases of the power spectrum in the precession, which requires a good control on the sample position in the field,

365   and a recommended density of sampling of 6-10 samples per precession cycle, depending on the uncertainty of the sample position.

Also in the evaluation of the relative contribution of precession and obliquity-related climatic forcing, an accurate assessment of the respective spectral power is essential (Ghirardi et al., 2014; Martinez et al., 2013; Weedon et al., 2004). Notably, whenever obliquity cycles are expressed more

370   manifestly compared to precession cycles, this has been interpreted as a reflection of important climate dynamics and feedback mechanisms at high latitudes (Ruddiman and McIntyre, 1984), the build-up and decay of quasi-stable carbon reservoirs (Laurin et al., 2015), or direct obliquity forcing at tropical latitudes (Bosmans et al., 2015; Park and Oglesby, 1991). A robust evaluation of the rela-

tive contribution of precession and obliquity requires at least that no bias occurs from the generation

375 of the depth series, which includes the sampling procedure. Once again, a good control of the sample position accompanied by a high density of sampling will importantly improve interpretations of the relative contributions of the precession and obliquity on the spectrum, which will in turn help making accurate palaeoclimatic interpretations.

8 Conclusions

380 Errors made during the measurement of the stratigraphic position of a sample significantly affect the power spectrum of depth series. We present a method to assess the impact of such errors that is compatible with different techniques for spectral analysis. Our method is based on a Monte-Carlo procedure that randomises the sample steps of the depth series, using a gamma distribution. Such a distribution preserves the stratigraphic order of samples, and allows controls on the mean and

385 the variance of the distribution of sample steps after randomisation. The simulations presented in this paper show that the gamma distribution of sample steps realistically simulates errors that are generally made during the measurement of sample positions. The three case studies presented in this paper all show a strong decrease in the power spectrum at high frequencies. With 5% stratigraphic uncertainty, the power spectrum is significantly affected in frequencies above 37% of the Nyquist

390 frequency. With 10% uncertainty, the power spectrum is noticeably different in frequencies above 22% of the Nyquist frequency. With 15% uncertainty, significant relative changes in power occur in frequencies above 15% of the Nyquist frequency. Simulations were performed on two geological datasets sampled with a density of 5 samples per precession cycle. These simulations show that with 10% uncertainty, the power of the precession band is decreased by 30-50%. Robust reconstruction

395 of the power spectrum in the entire Milankovitch band requires a robust control of the sample step on the field, and requires a high density of sampling. To avoid any dispersion of the power spectrum in the precession band, we suggest taking at least 6-10 samples per precession cycle depending on the level of uncertainty in the sample position.

Acknowledgements. ERC Consolidator Grant "EarthSequencing" (Grant Agreement No. 617462) funded this
400 project. Anna-Joy Drury is acknowledged for English-proof reading.

References

Bosmans, J. H. C., Hilgen, F. J., Tuenter, E., and Lourens, L. J.: Obliquity forcing of low-latitude climate, Climate of the Past, 11, 1335–1346, doi:10.5194/cp-11-1335-2015, http://www.clim-past.net/11/1335/2015/, 2015.

405 Boulila, S., Charbonnier, G., Galbrun, B., and Gardin, S.: Climatic precession is the main driver of Early Cretaceous sedimentation in the Vocontian Basin (France): Evidence from the Valanginian Orpierre succession, Sedimentary Geology, 324, 1–11, 2015.

Bulot, L. G., Thieuloy, J. P., Eric, B., and Klein, J.: Le cadre stratigraphique du Valanginien supérieur et de l'Hauterivien du Sud-Est de la France: définition des biochronozones et caractérisation de nouveaux biohori-

410 zons, Géologie Alpine, 68, 13–56, 1992.

Burgin, T. A.: The Gamma Distribution and Inventory Control, Operational Research Quarterly, pp. 507–525, 1975.

De Vleeschouwer, D. and Parnell, A. C.: Reducing time-scale uncertainty for the Devonian by integrating astrochronology and Bayesian statistics, Geology, 42, 491–494, doi:10.1130/G35618.1, http://geology.

415 gsapubs.org/content/42/6/491.abstract, 2014.

De Vleeschouwer, D., Boulvain, F., Da Silva, A.-C., Pas, D., Labaye, C., and Claeys, P.: The astronomical calibration of the Givetian (Middle Devonian) timescale (Dinant Synclinorium, Belgium), Geological Society, London, Special Publications, 414, doi:10.1144/SP414.3, http://sp.lyellcollection.org/content/early/2014/11/20/SP414.3.abstract, 2014.

420 Ghirardi, J., Deconinck, J.-F., Pellenard, P., Martinez, M., Bruneau, L., Amiotte-Suchet, P., and Pucéat, E.: Multi-proxy orbital chronology in the aftermath of the Aptian Oceanic Anoxic Event 1a: Palaeoceanographic implications (Serre Chaitieu section, Vocontian Basin, SE France), Newsletters on Stratigraphy, 47, 247–262, doi:10.1127/0078-0421/2014/0046, 2014.

Hagelberg, T. K., Pisias, N. G., Shackleton, N. J., Mix, A. C., and Harris, S. E.: Refinement of a high-resolution,

425 continuous sedimentary section for studying equatorial Pacific Ocean paleoceanography, Leg 138, in: Proceedings of the Ocean Drilling Program, Scientific Results, 138, edited by Pisias, N. G., Mayer, L. A., Janecek, T. R., Palmer-Julson, A., and van Andel, T. H., College Station, Tex.: Ocean Drilling Program, Texas A & M University, College Station, Texas, 1995.

Hinnov, L. A.: Cyclostratigraphy and its revolutionizing applications in the earth and planetary sciences, Geo-

430 logical Society of America Bulletin, 125, 1703–1734, doi:10.1130/B30934.1, http://gsabulletin.gsapubs.org/content/125/11-12/1703.abstract, 2013.

Hinnov, L. A., Schulz, M., and Yiou, P.: Interhemispheric space-time attributes of the Dansgaard-Oeschger oscillations between 100 and 0 ka, Quaternary Science Reviews, 21, 1213 – 1228, doi:10.1016/S0277-3791(01)00140-8, http://www.sciencedirect.com/science/article/pii/S0277379101001408, 2002.

435 Huybers, P. and Wunsch, C.: A depth-derived Pleistocene age model: Uncertainty estimates, sedimentation variability, and nonlinear climate change, Paleoceanography, 19, doi:10.1029/2002PA000857, http://dx.doi.org/10.1029/2002PA000857, 2004.

Laurin, J., Meyers, S. R., Uličný, D., Jarvis, I., and Sageman, B. B.: Axial obliquity control on the greenhouse carbon budget through middle- to high-latitude reservoirs, Paleoceanography, 30, 133–149,

440 doi:10.1002/2014PA002736, http://dx.doi.org/10.1002/2014PA002736, 2015.

Lomb, N. R.: Least-squares frequency analysis of unequally spaced data, Astrophysics and Space Science, 39, 447–462, doi:10.1007/BF00648343, http://dx.doi.org/10.1007/BF00648343, 1976.

Mann, M. E. and Lees, J. M.: Robust estimation of background noise and signal detection in climatic time series, Climatic Change, 33, 409–445, doi:10.1007/BF00142586, 1996.

445   Martinez, M. and Dera, G.: Orbital pacing of carbon fluxes by a ~9-My eccentricity cycle during the Mesozoic, Proceedings of the National Academy of Sciences, 112, 12 604–12 609, doi:10.1073/pnas.1419946112, http://www.pnas.org/content/112/41/12604.abstract, 2015.

Martinez, M., Deconinck, J.-F., Pellenard, P., Reboulet, S., and Riquier, L.: Astrochronology of the Valanginian Stage from reference sections (Vocontian Basin, France) and palaeoenvironmental impli-

450   cations for the Weissert Event, Palaeogeography, Palaeoclimatology, Palaeoecology, 376, 91 – 102, doi:10.1016/j.palaeo.2013.02.021, http://www.sciencedirect.com/science/article/pii/S0031018213000977, 2013.

Martinez, M., Deconinck, J.-F., Pellenard, P., Riquier, L., Company, M., Reboulet, S., and Moiroud, M.: Astrochronology of the Valanginian–Hauterivian stages (Early Cretaceous): Chronological relationships be-

455   tween the Paraná–Etendeka large igneous province and the Weissert and the Faraoni events, Global and Planetary Change, 131, 158 – 173, doi:10.1016/j.gloplacha.2015.06.001, http://www.sciencedirect.com/science/article/pii/S0921818115001113, 2015.

Matys Grygar, T., Mach, K., Schnabl, P., Pruner, P., Laurin, J., and Martinez, M.: A lacustrine record of the early stage of the Miocene Climatic Optimum in Central Europe from the Most Basin, Ohře (Eger) Graben,

460   Czech Republic, Geological Magazine, 151, 1013–1033, doi:10.1017/S0016756813001052, http://journals.cambridge.org/article_S0016756813001052, 2014.

Meyers, S. R.: Astrochron: An R Package for Astrochronology, http://cran.r-project.org/package=astrochron, 2014.

Moiroud, M., Martinez, M., Deconinck, J.-F., Monna, F., Pellenard, P., Riquier, L., and Company, M.: High-

465   resolution clay mineralogy as a proxy for orbital tuning: Example of the Hauterivian–Barremian transition in the Betic Cordillera (SE Spain), Sedimentary Geology, 282, 336 – 346, doi:10.1016/j.sedgeo.2012.10.004, http://www.sciencedirect.com/science/article/pii/S003707381200293X, 2012.

Moore, M. I. and Thomson, P. J.: Impact of jittered sampling on conventional spectral estimates, Journal of Geophysical Research: Oceans (1978–2012), 96, 18 519–18 526, 1991.

470   Mudelsee, M.: TAUEST: a computer program for estimating persistence in unevenly spaced weather/climate time series, Computers & Geosciences, 28, 69–72, 2002.

Park, J. and Oglesby, R. J.: Milankovitch rhythms in the Cretaceous: A GCM modelling study, Palaeogeography, Palaeoclimatology, Palaeoecology, 90, 329 – 355, doi:10.1016/S0031-0182(12)80034-4, http://www.sciencedirect.com/science/article/pii/S0031018212800344, 1991.

475   Pas, D., Da Silva, A. C., Devleeschouwer, X., De Vleeschouwer, D., Labaye, C., Cornet, P., Michel, J., and Boulvain, F.: Sedimentary development and magnetic susceptibility evolution of the Frasnian in Western Belgium (Dinant Synclinorium, La Thure section), Geological Society, London, Special Publications, 414, doi:10.1144/SP414.7, http://sp.lyellcollection.org/content/early/2014/12/01/SP414.7.abstract, 2014.

Reboulet, S. and Atrops, F.: Comments and proposals about the Valanginian-Lower Hauterivian ammonite

480   zonation of south-eastern France, Eclogae Geologicae Helvetiae, 92, 183–198, 1999.

Ruddiman, W. F. and McIntyre, A.: Ice-age thermal response and climatic role of the surface At-
lantic Ocean, 40°N to 63°N, Geological Society of America Bulletin, 95, 381–396, doi:10.1130/0016-
7606(1984)95<381:ITRACR>2.0.CO;2, http://gsabulletin.gsapubs.org/content/95/4/381.abstract, 1984.

Scargle, J. D.: Studies in astronomical time series analysis. II-Statistical aspects of spectral analysis of unevenly
485   spaced data, The Astrophysical Journal, 263, 835–853, doi:10.1086/160554, 1982.

Schulz, M. and Mudelsee, M.: REDFIT: estimating red-noise spectra directly from unevenly spaced pale-
oclimatic time series, Computers & Geosciences, 28, 421 – 426, doi:10.1016/S0098-3004(01)00044-9,
http://www.sciencedirect.com/science/article/pii/S0098300401000449, 2002.

Thomson, D. J.: Spectrum estimation and harmonic analysis, Proceedings of the IEEE, 70, 1055–1096,
490   doi:10.1109/PROC.1982.12433, 1982.

Thomson, D. J.: Quadratic-Inverse Spectrum Estimates: Applications to Palaeoclimatology, Philosophical
Transactions of the Royal Society of London A: Mathematical, Physical and Engineering Sciences, 332,
539–597, doi:10.1098/rsta.1990.0130, 1990.

Weedon, G. P. and Jenkyns, H. C.: Cyclostratigraphy and the Early Jurassic timescale: Data from the
495   Belemnite Marls, Dorset, southern England, Geological Society of America Bulletin, 111, 1823–1840,
doi:10.1130/0016-7606(1999)111<1823:CATEJT>2.3.CO;2, http://gsabulletin.gsapubs.org/content/111/12/
1823.abstract, 1999.

Weedon, G. P., Coe, A. L., and Gallois, R. W.: Cyclostratigraphy, orbital tuning and inferred productivity for the
type Kimmeridge Clay (Late Jurassic), Southern England, Journal of the Geological Society, 161, 655–666,
500   doi:10.1144/0016-764903-073, http://jgs.lyellcollection.org/content/161/4/655.abstract, 2004.

Zeeden, C., Meyers, S. R., Lourens, L. J., and Hilgen, F. J.: Testing astronomically tuned age models, Paleo-
ceanography, 30, 369–383, doi:10.1002/2014PA002762, 2015.
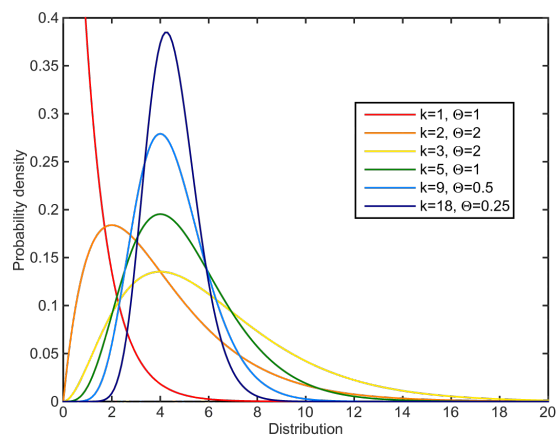
Figure 1. Gamma probability density functions (PDF). All Gamma PDF's have a positive support, which is a crucial characteristic to realistically simulate sample steps. The gamma density probability functions were generated with the Matlab gampdf function.
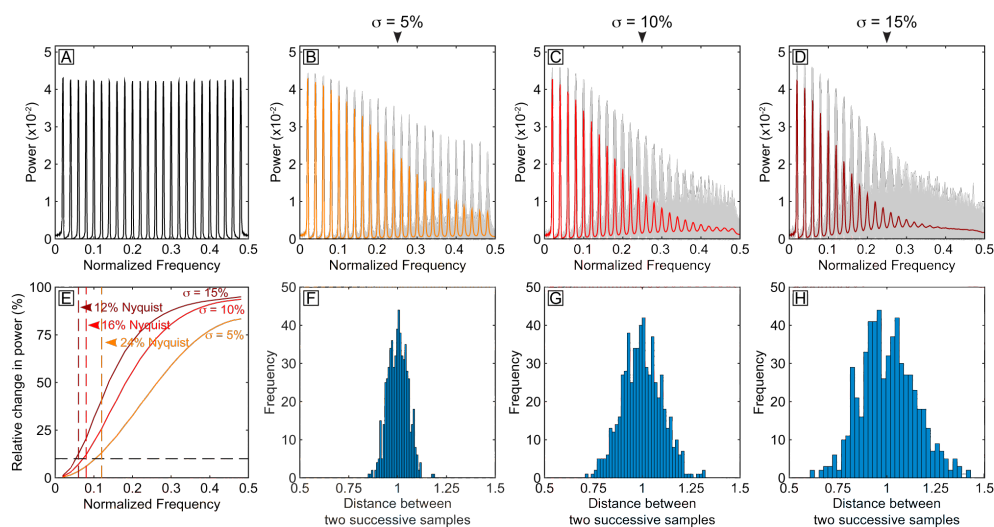
Figure 2. Effect of the gamma-law randomised sample steps on the 2π-MTM spectra of the series of sum of pure sinusoids. 2π-MTM spectrum of the series sum of sinusoids: (A.) without sample step randomisation; (B., C. and D.) with a sample step randomisation showing a standard deviation σ of respectively 5%, 10% and 15% of the average sample step of the series. For each simulation shown in B., C. and D., the grey lines represent the spectrum of each of the simulation and the red, orange and brown curve represent the average spectrum. (E.) Evolution of the relative change in power of the spectral peaks from frequency 0 to the Nyquist frequency observed in each of the simulations. The black dash line represents the threshold of 10% of misfit. The brown, red and orange vertical dash lines represent the frequency for which the threshold of 10% of misfit is reached. (F., G. and H.) Distribution of the randomised sample steps after one of the Monte-Carlo simulations.
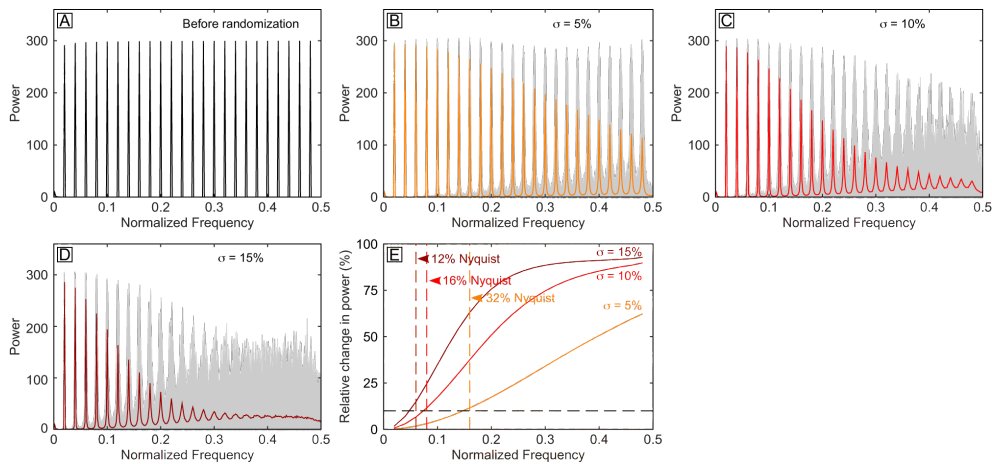
Figure 3. Effect of the gamma-law randomised sample steps of the Lomb-Scargle spectra of the series of sum of pure sinusoids. Lomb-Scargle spectra of the series sum of sinusoids: (A.) without sample step randomisation; (B., C. and D.) with a sample step randomisation showing a standard deviation σ of respectively 5%, 10% and 15% of the average sample step of the series. (E.) Evolution of the relative change in power of the spectral peaks from frequency 0 to the Nyquist frequency observed in each of the simulations.
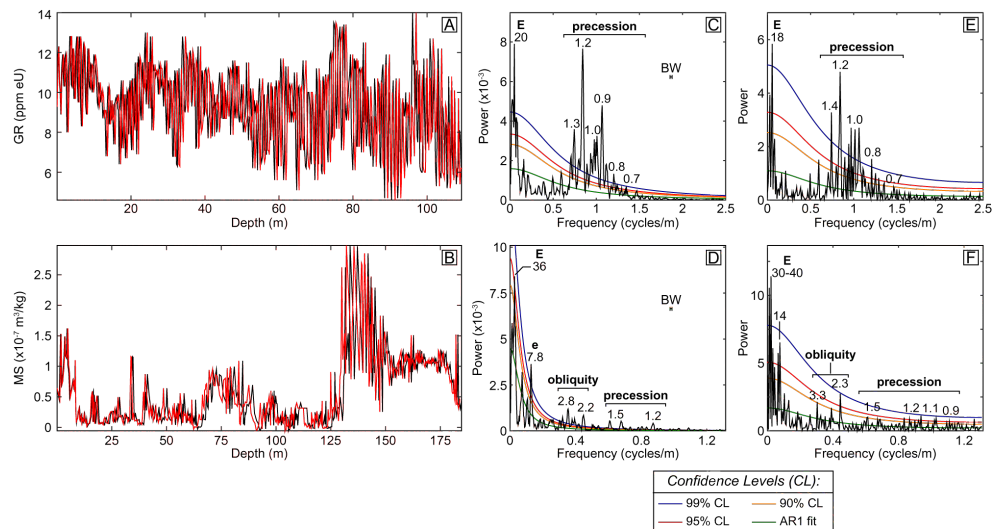
Figure 4. Superposition of the raw data (in black) to one simulation of gamma-law-randomised sample steps with an uncertainty of 15% (in red) for (A.) the La Charce series, and (B.) the La Thure series. Notice that the stratigraphic order of the points remains unchanged after the randomisation process. 2π-MTM spectra of (C.) the La Charce section and (D.) the La Thure section. REDFIT Lomb-Scargle spectrum of (E.) the La Charce section and (F.) the La Thure section.
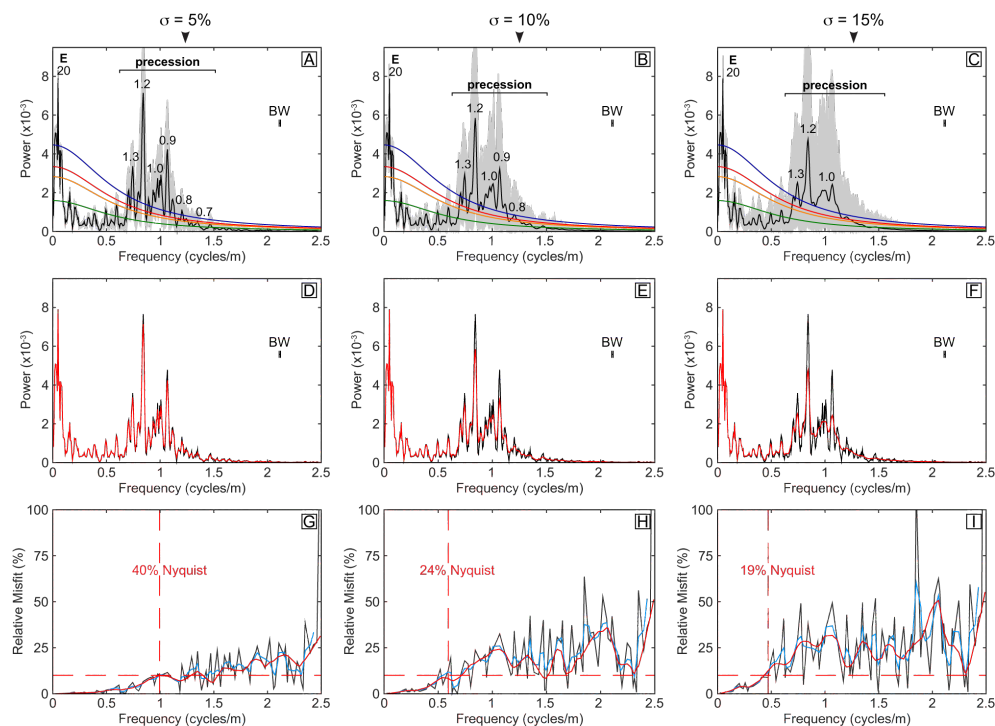
Figure 5. Effect of the gamma-law randomisation of the sample step on the 2π-MTM spectrum of the gamma-ray series from the La Charce section. (A., B., C.) 2π-MTM spectrum of the series sum of sinusoids with a sample step randomisation showing a standard deviation σ of respectively 5%, 10% and 15% of the average sample step of the series. The grey lines represent the spectrum of each of the 1000 simulations and the black curve represents the average spectrum. The same confidence levels as in Fig. 4C are reported. (D., E., F.) Superposition of the 2π-MTM spectrum before randomisation (in black) and the average spectrum after the 1000 simulations (in red). (G., H. and I.) Evolution of the relative change in power from frequency 0 to the Nyquist frequency for each of the simulations. The horizontal red dash lines represent the threshold of 10% of misfit. The vertical red dash lines represent the frequency for which the threshold of 10% of misfit is reached. The blue line represents the 5-points Gaussian moving average, and the solid red line represents the 10%-LOWESS regression. BW: BandWidth. The colour code of the confidence levels is the same as in Fig. 4.
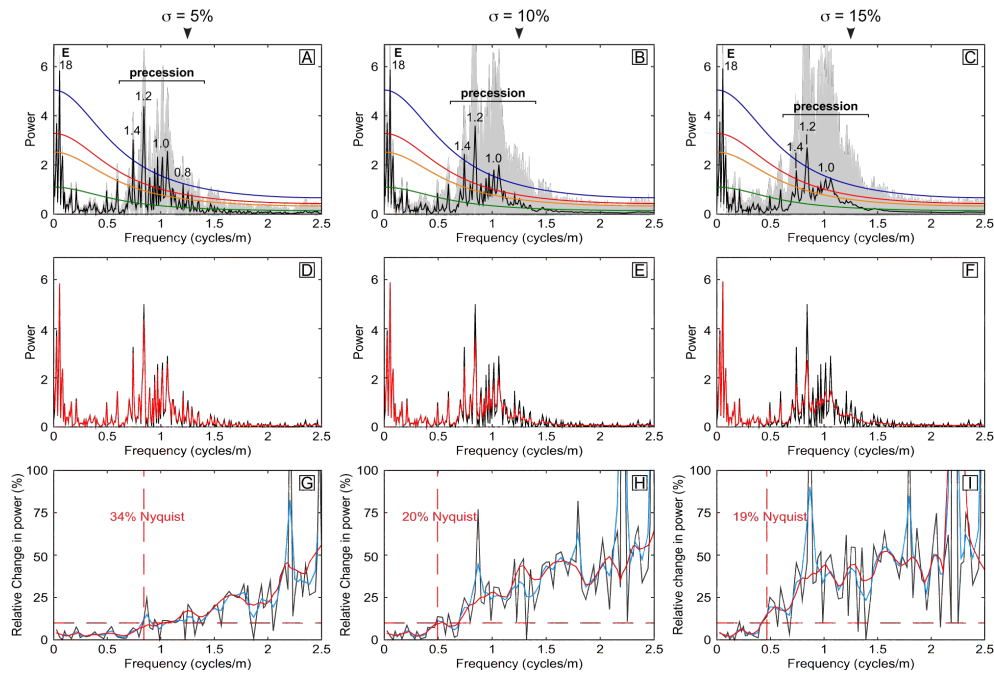
Figure 6. Effect of the gamma-law randomisation of the sample step on the REDFIT spectrum of the gamma-ray series from the La Charce section. (A., B., C.) REDFIT Lomb-Scargle spectra of the gamma-ray series with a sample step randomisation showing a standard deviation σ of respectively 5%, 10% and 15% of the average sample step of the series. The grey lines represent the spectrum of each simulation and the black curve represents the average spectrum. The same confidence levels as in Fig. 4E are reported. (D., E., F.) Superposition of the REDFIT Lomb-Scargle spectrum before randomisation (in black) and the average spectrum after the 1000 simulations (in red). (G., H., I.) Evolution of the relative change in power from frequency 0 to the Nyquist frequency for each of the simulations. The horizontal red dash lines represent the threshold of 10% of misfit. The vertical red dash lines represent the frequency for which the threshold of 10% of misfit is reached. The blue line represents the 5-points Gaussian moving average, and the solid red line represents the 10%-LOWESS regression. The colour code of the confidence levels is the same as in Fig. 4.
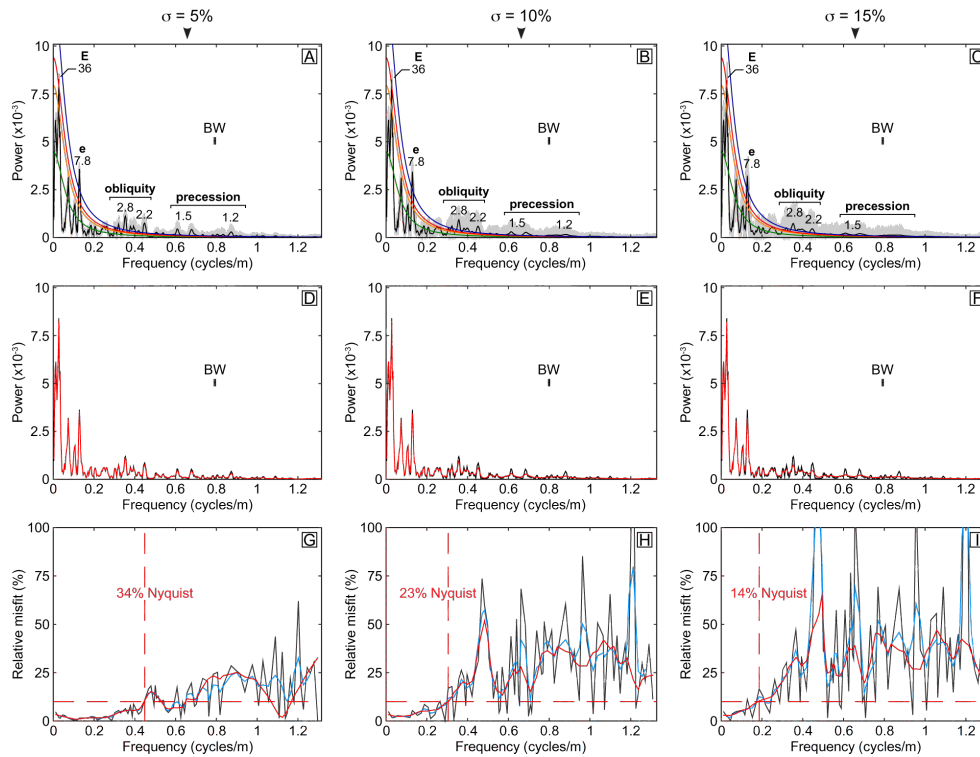
Figure 7. Effect of the gamma-law randomisation of the sample step on the 2π-MTM spectrum of the gamma-ray series from the La Thure section. (A., B., C.) 2π-MTM spectrum of the series sum of sinusoids with a sample step randomisation showing a standard deviation σ of respectively 5%, 10% and 15% of the average sample step of the series. The grey lines represent the spectrum of each of the 1000 simulations and the black curve represents the average spectrum. The same confidence levels as in Fig. 4D are reported. (D., E., F.) Superposition of the 2π-MTM spectrum before randomisation (in black) and the average spectrum after the 1000 simulations (in red). (G., H. and I.) Evolution of the relative change in power from frequency 0 to the Nyquist frequency for each of the simulations. The horizontal red dash lines represent the threshold of 10% of misfit. The vertical red dash lines represent the frequency for which the threshold of 10% of misfit is reached. The blue line represents the 5-points Gaussian moving average, and the solid red line represents the 10%-LOWESS regression. BW: BandWidth. The colour code of the confidence levels is the same as in Fig. 4.
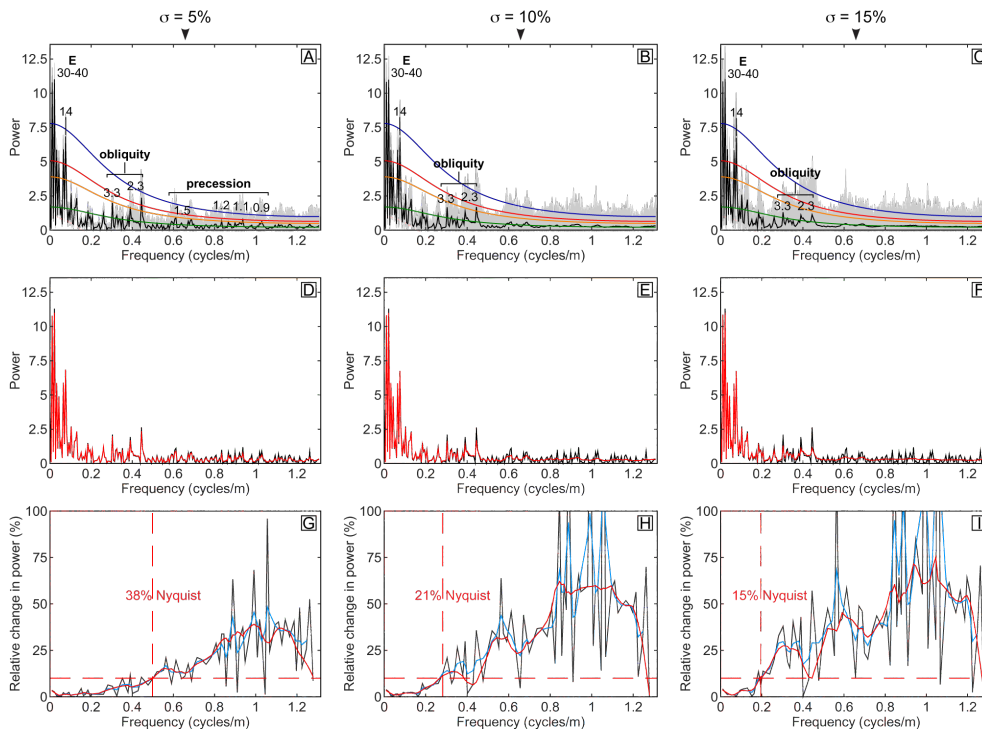
Figure 8. Effect of the gamma-law randomisation of the sample step on the REDFIT spectrum of the gamma-ray series from the La Thure section. (A., B., C.) REDFIT Lomb-Scargle spectra of the gamma-ray series with a sample step randomisation showing a standard deviation σ of respectively 5%, 10% and 15% of the average sample step of the series. The grey lines represent the spectrum of each simulation and the black curve represents the average spectrum. The same confidence levels as in Fig. 4F are reported. (D., E., F.) Superposition of the REDFIT Lomb-Scargle spectrum before randomisation (in black) and the average spectrum after the 1000 simulations (in red). (G., H., I.) Evolution of the relative change in power from frequency 0 to the Nyquist frequency for each of the simulations. The horizontal red dash lines represent the threshold of 10% of misfit. The vertical red dash lines represent the frequency for which the threshold of 10% of misfit is reached. The blue line represents the 5-points Gaussian moving average, and the solid red line represents the 10%-LOWESS regression. The colour code of the confidence levels is the same as in Fig. 4.